Fabrication and electrical properties of axial and radial GaAs nanowire pn junction diode arrays*

Li Jun-Shuai(李军帅), Zhang Xia(张 霞)†, Yan Xin(颜 鑫), Chen Xiong(陈 雄), Li Liang(李 亮), Cui Jian-Gong(崔建功), Huang Yong-Qing(黄永清), and Ren Xiao-Min(任晓敏)

State Key Laboratory of Information Photonics and Optical Communications, Beijing University of Posts and Telecommunications, Beijing 100876, *China*

(Received 11 March 2014; revised manuscript received 17 May 2014; published online 10 October 2014)

We report on the fabrications and characterizations of axial and radial GaAs nanowire pn junction diode arrays. The nanowires are grown on n-doped GaAs (111)B substrates using the Au-catalyzed vapor–liquid–solid mechanism by metal–organic chemical vapor deposition (MOCVD). Diethyl–zinc and silane are used as p- and n-type dopant precursors, respectively. Both the axial and radial diodes exhibit diode-like *J*–*V* characteristics and have similar performances under forward bias. Under backward bias, the axial diode has a large leakage current, which is attributed to the bending of the pn junction interface induced by two doping mechanisms in Au-catalyzed nanowires. The low leakage current and high rectification ratio make the radial diode more promising in electrical and optoelectronic devices.

Keywords: pn junction diode, GaAs nanowire, MOCVD

PACS: 85.30.Kk, 81.07.–b, 81.07.Gf **DOI:** 10.1088/1674-1056/23/12/128503

1. Introduction

Semiconductor nanowires (NWs) have attracted much attention in recent years due to their unique advantages such as the bottom–up paradigm, enhanced strain relaxations, and advanced electrical and optical properties.[1–4] As an important structure, NW pn junctions have been widely studied and applied in a lot of nano-electronic and nano-optoelectronic devices including bipolar transistors,[5,6] optical sources,[7] photodetectors,[8] and solar cells.[9–11] There are mainly two types of NW pn junctions: axial junction[8,12–14] and radial junction.[9,10] The axial junction is similar to the planar junction in which the junction interface is vertical to the growth direction. The radial junction is formed by surrounding the doped core with a shell of the opposite doping type, which enables carrier extraction across the radius of the NW, while a long axial length of the NW permits high optical absorption.

Large-scale vertically aligned NW pn junction arrays are particularly promising in high-performance optoelectronic devices due to the light trapping mechanism. High-efficiency solar cells have been fabricated based on direct band gap III–V NW pn junction arrays.[7,9–11] In this work, we fabricate axial and radial GaAs nanowire pn junction diode arrays and study their electrical properties. Both the two diodes exhibit diode-like *I*–*V* characteristics. The radial diode has a lower leakage current and higher rectification ratio than the axial one, which is more promising in electrical and optoelectronic devices.

2. Experimental procedure

The growth was performed by using a Thomas Swan CCS-MOCVD system at a pressure of 100 Torr (1 Torr = 1.33322×10^2 Pa). The carrier was hydrogen. Trimethyl–gallium (TMGa) and arsine (AsH_3) were used as precursors. Silane (SiH_4) and diethyl–zinc (DEZn) were chosen as the sources for n-type and p-type doping, respectively. Au film with a thickness of 4 nm was deposited on the n-doped GaAs (111)B substrate by magnetron sputtering. The Au-coated substrate was loaded into the MOCVD reactor and annealed at 650 °C under AsH_3 ambient for 300 s to form Au–Ga alloyed particles as the catalyst. For the axial junction, a lower n-type GaAs NW section was firstly grown at 440 °C for 300 s, then the upper p-type section was grown at the same temperature for 300 s. For the radial junction, an n-type NW core was firstly grown at 440 °C for 400 s. After that, the temperature was raised to 560 °C, p-type GaAs shell was subsequently grown for 100 s. During growth, the flow rates of TMGa, AsH_3, SiH_4, and DEZn were 14.4 sccm, 100 sccm, 40 sccm, 40 sccm respectively.

The schematics and scanning electron microscopy (SEM) images of NWs are shown in Fig. 1. From Fig. 1(b), we can see that the axial pn NWs show kinking, which is attributed

*Project supported by the National Natural Science Foundation of China (Grant Nos. 61376019 and 61020106007), the Specialized Research Fund for the Doctoral Program of Higher Education of China (Grant No. 20120005110011), the Natural Science Foundation of Beijing (Grant No. 4142038), the 111 Program of China (Grant No. B07005), and the Fund of the State Key Laboratory of Information Photonics and Optical Communications (Beijing University of Posts and Telecommunications).

†Corresponding author. E-mail: xzhang@bupt.edu.cn

© 2014 Chinese Physical Society and IOP Publishing Ltd

to the incorporation of Zn into the Au particle during the p-type nanowire growth.[15] The total length of the axial pn NW is about 5.8 μm. The length of the n-doped section is determined to be 4.2 μm from an independent growth of pure n-doped NWs under the same condition. Thus the p-doped NW section is determined to be 1.6 μm, which indicates an effective growth time of 114 s due to splitting of catalyst drop and kinking.[15] Figure 1(d) shows the SEM image of radial pn NWs. It can be seen that these NWs remain straight and uniform, no kinging is observed. This is because the p-type shell directly deposits on the NW surface under high temperature and the incorporation of Zn into Au is suppressed. The total length of NWs is about 5.4 μm and the thickness of the p-doped shell is 50 nm. A short "neck" with a smaller diameter is observed under the Au catalyst, which is considered to be formed during the shell growth. The p-doped "neck" is helpful to avoid contact between the top electrode and n-doped NW cores.

The fabrication process of NW array pn junction diodes is shown in Fig. 2. Firstly, the NW arrays were covered with polyimide (PI) by spin casting. For the axial array, PI-5 was spun onto the sample without dilution at 2000 rpm for 4 min. For radial arrays, PI-5 was diluted four times and spun at 2000 rpm for 4 min. After spinning, the two samples were hard-cured overnight. To expose the NW tips for electrode contact, the samples were placed in an oxygen plasma reactive ion etch chamber to remove the polyimide from the tips of the NWs. A top contact consisting of Pt/Ti/Pt/Au was then deposited on the NW tips by magnetron sputtering. A back contact consisting of Pt/Ti/Pt/Au was deposited on the backside of the substrate.

Figure 3 shows the SEM images of axial and radial NW arrays after covering PI as well as after depositing electrodes. Figure 3(a) shows the 70 °-tilted SEM image of the axial array. We can see that all the NWs are covered with a planar PI film. Figure 3(b) shows a cross-sectional SEM image of the array with a single NW. It can be seen clearly that the tip is exposed. The exposed length is about 200 nm, which can maintain a good contact between the p-doped NW and the top electrode while avoiding the contact between the lower n-doped NW and the electrode. Figure 3(c) shows the SEM image of axial array after depositing electrode. The electrode is in the form of a uniform film and connects all the nanowire tips. From the high magnification image, the electrode thickness is determined to be 70 nm. For the radial sample, the PI film is thinner and the exposed length is much longer. This is helpful to maintain a large contact area with electrodes, as shown in Figs. 3(d)–3(f).

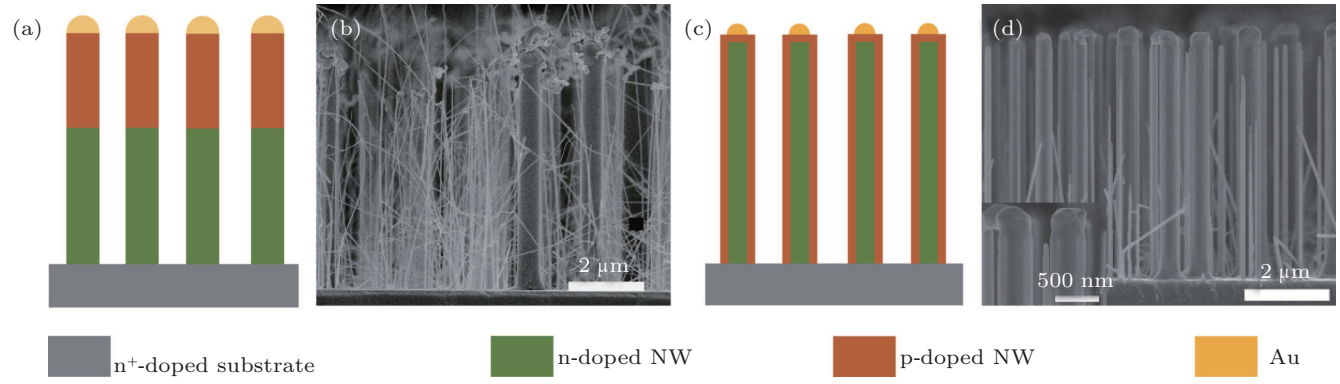


Fig. 1. (color online) Schematics and SEM images of axial and radial GaAs NW pn junction arrays.

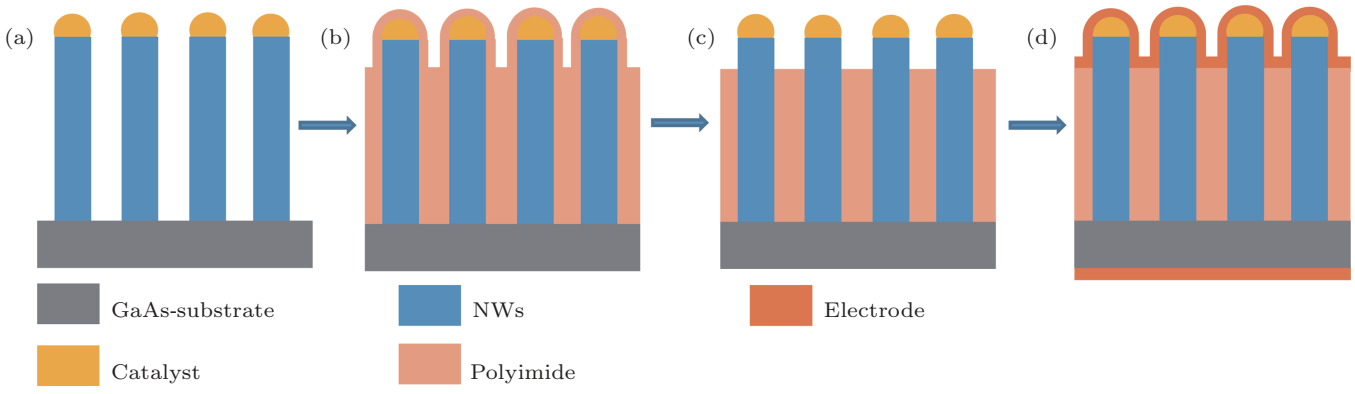


Fig. 2. (color online) Schematic diagram of the device fabrication process: (a) as-grown NW pn junction array, (b) NW arrays after spinning PI, (c) NW arrays after etching, and (d) NW arrays after depositing electrodes.

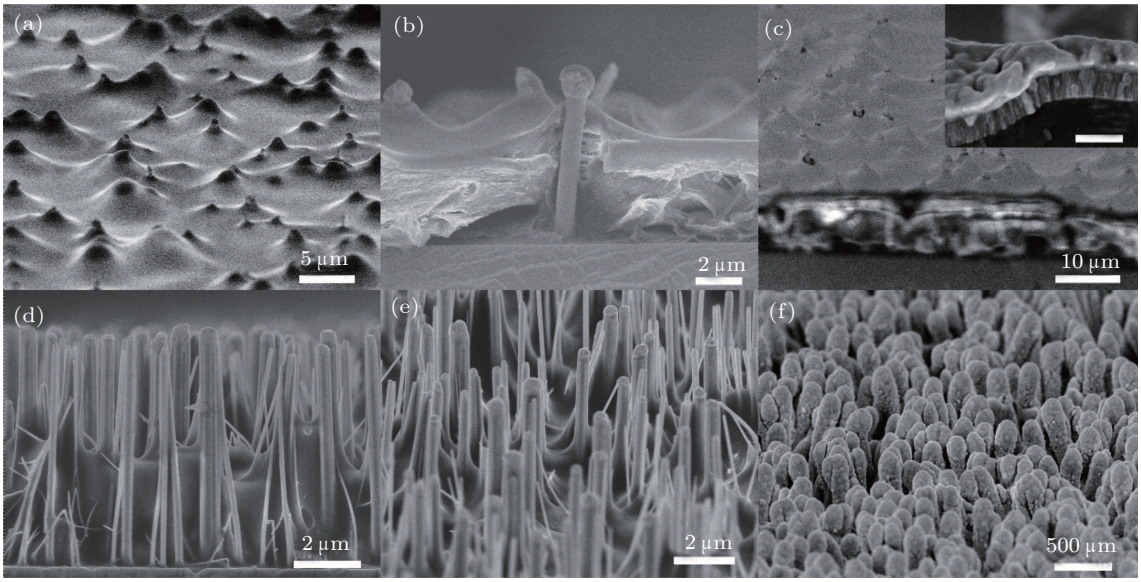


Fig. 3. SEM images of axial ((a)–(c)) and radial ((d)–(f)) NW pn arrays with PI and electrodes.

3. Results and discussion

The electrical properties of devices are studied by using a Keithley 2636A digital source-meter. Figure 4(a) shows the current density–voltage (J–V) characteristics of the devices. Both the axial and radial diodes exhibit diode-like J–V characteristics.[16] Under forward bias, the characteristics of the two diodes are similar. The onset voltage is about 0.4 V, which can be determined from the J–V curve plotted in semi-logarithm. In the range of 0 V–0.4 V, the intrinsic ideality factors are 2 and 2.5 for the axial and radial diodes, respectively, which are similar to those of the GaAs nanowire diodes reported previously.[17] The series resistances are 122 Ω·mm^2 and 155 Ω·mm^2 for the axial and radial diodes, respectively, as determined from curves beyond the turn-on voltage. The large series resistance may be attributed to the contact of the upper electrode to a thick surface depletion region of NWs with a low doping level.[12,18–20]

Under backward bias, the axial diode has a much larger leakage current density than its radial counterpart. For example, the leakage current density at −2 V of the axial diode is 1.92 mA/mm^2, while for the radial diode, it is only 0.26 mA/mm^2. Moreover, the leakage current of the axial diode increases much faster than that of the radial one and exhibits some indications of breakdown. Figure 4(b) shows the rectification ratio of diodes. The rectification ratio of the radial diode is several times higher than the axial one. For example, the rectification ratios at 1 V are 60 and 14 for the radial and axial diode, respectively. Considering the similar forward conduction currents, the low rectification ratio of the axial diode is obviously attributed to the large leakage current.

The difference in the leakage current between axial and radial diodes is probably attributed to the difference in doping mechanism between the two types of pn structures. As has been reported, there are two doping mechanisms in VLS grown nanowires: doping through side facet deposition and doping through the droplet which is illustrated as Fig. 5(a).[21]

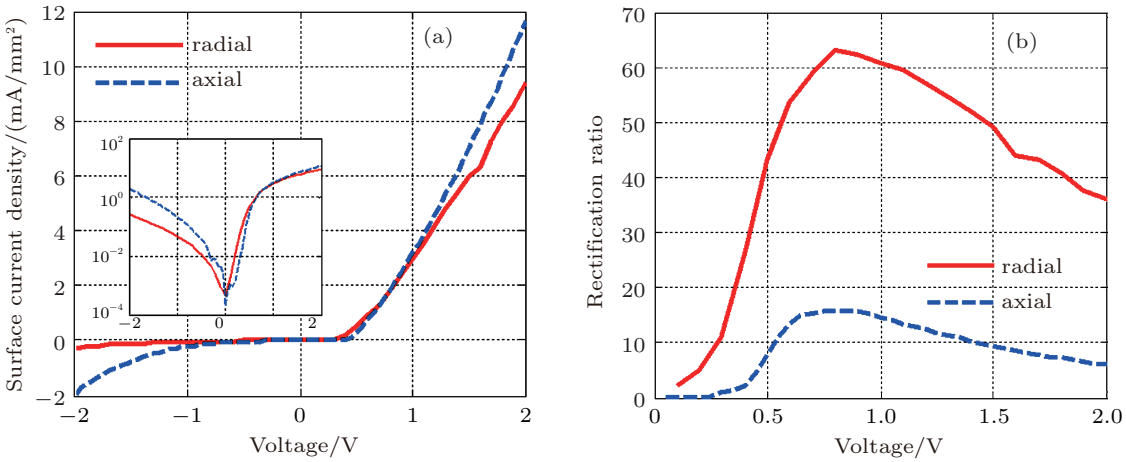


Fig. 4. (color online) Electrical properties of axial and radial NW pn array diodes: (a) J–V characteristics of the axial and radial devices. The inset shows the J–V curves in semi-logarithm. (b) Rectification curves of the devices.

For the radial diode, high temperature shell growth means the former mechanism dominates the procedure, which leads to a uniform doping concentration along the NW and a smooth pn junction interface. Considering the axial diode, radial growth always occurs during the growth of the p-doped section, though it might be thousands of times slower than the axial growth. This means that both of the two mechanisms contribute to the doping of a p-doped NW, resulting in different doping concentrations in the center and external part of the NW. The concentration difference may lead to a bending of the junction interface, as illustrated in Fig. 5(b). The interface bending can result in a low breakdown voltage, and the leakage current can increase rapidly at a small backward voltage.[18,22]

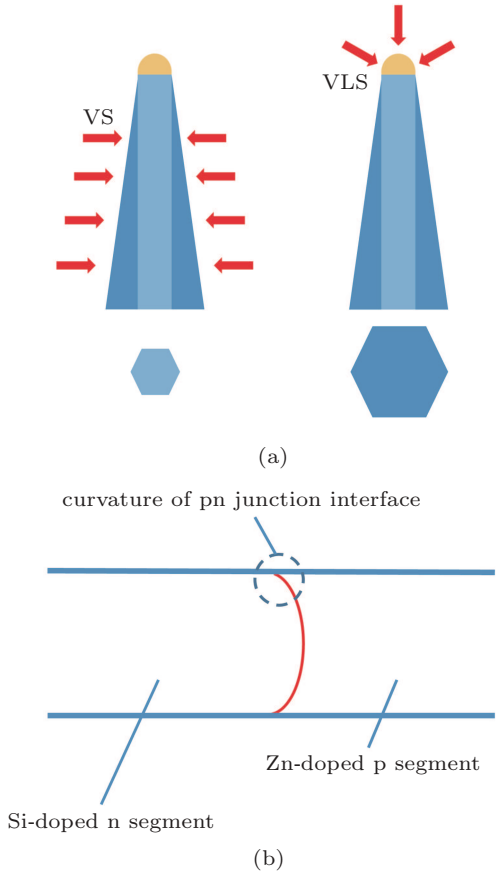


Fig. 5. (color online) Schematics of (a) doping mechanisms in Au-catalyzed VLS nanowires and (b) bending of the pn junction interface.

4. Conclusion

In this paper, we fabricated axial and radial GaAs nanowire pn junction diode arrays and studied their electrical properties. The axial NW array exhibits kinking due to the incorporation of Zn into the Au particle, while the radial array remains straight and uniform. Both the axial and radial diodes exhibit diode-like J–V characteristics and have similar performances under forward bias while there exists a large series resistance mainly due to surface depletion. Under backward bias, the axial diode has a large leakage current, which may be caused by the bending of the pn junction interface induced by two doping mechanisms in Au-catalyzed nanowires. The low leakage current and high rectification ratio make the radial diode more promising in electrical and optoelectronic devices.

References

[1] Tian B, Kempa T J and Lieber C M 2009 *Chem. Soc. Rev.* **38** 16
[2] Guo J W, Huang H, Ren X M, Yan X, Cai S W, Guo X, Huang Y Q, Wang Q, Zhang X and Wang W 2011 *Chin. Phys. Lett.* **28** 036101
[3] Lü X L, Zhang X, Liu X L, Yan X, Cui J G, Li J S, Huang Y Q and Ren X M 2013 *Chin. Phys. B* **22** 66101
[4] Yan X, Zhang X, Li J S, Lü X L, Ren X M and Huang Y Q 2013 *Chin. Phys. B* **22** 76102
[5] Cui Y and Lieber C M 2001 *Science* **291** 851
[6] Kucherlapati N S 2010 "Modeling of a Three-Layer Coated Nanowire Transistor" (MS Thesis) (University of Akron)
[7] Hersee S D, Fairchild M, Rishinaramangalam A K, Ferdous M S, Zhang L, Varangis P M, Swartzentruber B S and Talin A A 2009 *Electron. Lett.* **45** 75
[8] Yang C, Barrelet C J, Capasso F and Lieber C M 2006 *Nano Lett.* **6** 2929
[9] Czaban J A, Thompson D A and Lapierre R R 2009 *Nano Lett.* **9** 148
[10] Mariani G, Scofield A C, Hung C H and Huffaker D L 2013 *Nat. Commun.* **4** 1497
[11] Wallentin J, Anttu N, Asoli D, Huffman M, Aberg I, Magnusson M H, Siefer G, Fuss-Kailuweit P, Dimroth F, Witzigmann B, Xu H Q, Samuelson L, Deppert K and Borgström M T 2013 *Science* **339** 1057
[12] Gutsche C, Lysov A, Regolin I, Münstermann B, Prost W and Tegude F J 2012 *J. Electron. Mater.* **41** 809
[13] Gutsche C, Niepelt R, Gnauck M, Lysov A, Prost W, Ronning C and Tegude F J 2012 *Nano Lett.* **12** 1453
[14] Hoffmann S, Bauer J, Ronning C, Stelzner T, Michler J, Ballif C, Sivakov V and Christiansen S H 2009 *Nano Lett.* **9** 1341
[15] Gutsche C, Regolin I, Blekker K, Lysov A, Prost W and Tegude F J 2009 *J. Appl. Phys.* **105** 024305
[16] Wang M, Wang D J, Wang R W and Li Y B 2014 *Chin. Phys. B* **23** 047301
[17] Lysov A, Offer M, Gutsche C, Regolin I, Topaloglu S, Geller M, Prost W and Tegude F J 2011 *Nanotechnology* **22** 085702
[18] Pierret R F 2010 *Semiconductor Device Fundamentals*, translated by Huang R and Wang Y (Beijing: Electronics Industry Press) pp. 183–198 & 250–253 (in Chinese)
[19] Chang C C, Chi C Y, Yao M Q, Huang N F, Chen C C, Theiss J, Bushmaker A W, LaLumondiere S, Yeh T W, Povinelli M L, Zhou C W, Dapkus P D and Cronin S B 2012 *Nano Lett.* **12** 4484
[20] Sager D, Gutsche C, Prost W, Tegude F J and Bacher G 2013 *J. Appl. Phys.* **113** 174303
[21] Dufouleur J, Colombo C, Garma T, Ketterer B, Uccelli E, Nicotra M and Morral A F 2010 *Nano Lett.* **10** 1734
[22] Sze S M and Gibbons G 1966 *Solid-State Electron.* **9** 831